

## Article

# Three-Step Process for Efficient Solar Cells with Boron-Doped Passivated Contacts

Saman Sharbaf Kalaghichi <sup>1,2,\*</sup>, Jan Hoß <sup>1</sup>, Jonathan Linke <sup>1</sup> , Stefan Lange <sup>3</sup>  and Jürgen H. Werner <sup>2</sup> 

<sup>1</sup> International Solar Energy Research Center Konstanz, Rudolf-Diesel-Straße 15, 78467 Konstanz, Germany; jan.hoss@isc-konstanz.de (J.H.); jonathan.linke@isc-konstanz.de (J.L.)

<sup>2</sup> Institute for Photovoltaics, University of Stuttgart, Pfaffenwaldring 47, 70569 Stuttgart, Germany; juergen.werner@ipv.uni-stuttgart.de

<sup>3</sup> Fraunhofer Center for Silicon Photovoltaics, Otto-Eißfeldt-Straße 12, 06120 Halle, Germany

\* Correspondence: saman.sharbaf@isc-konstanz.de

**Abstract:** Crystalline silicon (c-Si) solar cells with passivation stacks consisting of a polycrystalline silicon (poly-Si) layer and a thin interfacial silicon dioxide (SiO<sub>2</sub>) layer show high conversion efficiencies. Since the poly-Si layer in this structure acts as a carrier transport layer, high doping of the poly-Si layer is crucial for high conductivity and the efficient transport of charge carriers from the bulk to a metal contact. In this respect, conventional furnace-based high-temperature doping methods are limited by the solid solubility of the dopants in silicon. This limitation particularly affects p-type doping using boron. Previously, we showed that laser activation overcomes this limitation by melting the poly-Si layer, resulting in an active concentration beyond the solubility limit after crystallization. High electrically active boron concentrations ensure low contact resistivity at the (contact) metal/semiconductor interface and allow for the maskless patterning of the poly-Si layer by providing an etch-stop layer in an alkaline solution. However, the high doping concentration degrades during long high-temperature annealing steps. Here, we performed a test of the stability of such a high doping concentration under thermal stress. The active boron concentration shows only a minor reduction during SiN<sub>x</sub>:H deposition at a moderate temperature and a fast-firing step at a high temperature and with a short exposure time. However, for an annealing time  $t_{\text{anneal}} = 30$  min and an annealing temperature  $600\text{ °C} \leq T_{\text{anneal}} \leq 1000\text{ °C}$ , the high conductivity is significantly reduced, whereas a high passivation quality requires annealing in this range. We resolve this dilemma by introducing a second, healing laser reactivation step, which re-establishes the original high conductivity of the boron-doped poly-Si and does not degrade the passivation. After a thermal annealing temperature  $T_{\text{anneal}} = 985\text{ °C}$ , the reactivated layers show high sheet conductance ( $G_{\text{sh}}$ ) with  $G_{\text{sh}} = 24\text{ mS sq}$  and high passivation quality, with the implied open-circuit voltage ( $iV_{\text{OC}}$ ) reaching  $iV_{\text{OC}} = 715\text{ mV}$ . Therefore, our novel three-step process consisting of laser activation, thermal annealing, and laser reactivation/healing is suitable for fabricating highly efficient solar cells with p<sup>++</sup>-poly-Si/SiO<sub>2</sub> contact passivation layers.

**Keywords:** passivating contacts; poly-Si layers; laser activation; thermal stability; electrical deactivation; reactivation



**Citation:** Sharbaf Kalaghichi, S.; Hoß, J.; Linke, J.; Lange, S.; Werner, J.H. Three-Step Process for Efficient Solar Cells with Boron-Doped Passivated Contacts. *Energies* **2024**, *17*, 1319. <https://doi.org/10.3390/en17061319>

Academic Editor: Pham Duy Phong

Received: 26 January 2024

Revised: 5 March 2024

Accepted: 7 March 2024

Published: 9 March 2024



**Copyright:** © 2024 by the authors. Licensee MDPI, Basel, Switzerland. This article is an open access article distributed under the terms and conditions of the Creative Commons Attribution (CC BY) license (<https://creativecommons.org/licenses/by/4.0/>).

## 1. Introduction

Solar cells with passivated contacts are widely considered the future technology of solar cell production because of their superior passivation quality. Two main passivated contact technologies are silicon heterojunction (SHJ) cells and tunnel oxide passivated contact (TOPCon) solar cells. SHJ solar cells offer a good passivation quality with a high open-circuit voltage, but the necessity of low-temperature metallization and the scarcity of the required indium for indium tin oxide (ITO) create obstacles to large-scale industrialization [1]. On the contrary, the production capacity for TOPCon solar cells is quickly expanding [2] due to the fact that upgrading the production line from the current

industrially dominant passivated emitter rear cells (PERCs) to TOPCon requires only a few additional process steps [3]. TOPCon technology uses passivation layers consisting of a thin interfacial silicon dioxide ( $\text{SiO}_2$ ) layer and highly doped poly-silicon ( $\text{SiO}_2/\text{poly-Si}$ ). The present industrial TOPCon solar cells use a highly phosphorous-doped n-type poly-Si layer ( $\text{n}^+$ -poly-Si) fabricated by furnace-based processes for passivating rear-side contacts [4–6]. However, future, more advanced cell concepts with passivated contacts will also need p-type-doped poly-Si layers ( $\text{p}^+$ -poly-Si) in order to passivate both polarities. Such cells could be poly-Si passivated interdigitated back contact (IBC) solar cells and TOPCon cells with a  $\text{p}^+$ -poly-Si/ $\text{SiO}_2$  passivation layer on the front side. Compared to n-type doping, achieving high p-type doping in a poly-Si layer with conventional dopants such as boron is more challenging with conventional furnace-based processes due to the relatively low solid-state solubility  $s$  of boron in silicon, which amounts to  $s \approx 1 \times 10^{20} \text{ cm}^{-3}$  at  $1000 \text{ }^\circ\text{C}$  [7]. Furthermore, furnace-based processes do not allow such passivation layers to only be applied locally.

In a previous publication, we introduced a laser activation process resulting in poly-Si layers that are supersaturated with electrically active boron atoms beyond the solid solubility limit [8]. Due to the significantly higher diffusion coefficient ( $D$ ) of boron in molten Si compared to solid Si ( $D_l \approx 10^{-4} \text{ cm}^2/\text{s}$  in liquid [9],  $D_s \approx 10^{-11} \text{ cm}^2/\text{s}$  in solid at  $1150 \text{ }^\circ\text{C}$  [10]), the majority of boron atoms, including the electrically deactivated atoms, diffuse into the molten Si after a laser pulse melts the lightly furnace-doped  $\text{p}^+$ -poly-Si layer. When the laser pulse is finished, the molten silicon quickly recrystallizes and traps the boron atoms in the silicon lattice. Obviously, the boron atoms stay electrically active after crystallization at concentrations above the solubility limit [11,12].

For the production of highly efficient industrial Si solar cells, a high boron concentration in poly-Si layers beyond the conventional solid solubility promises the following advantages:

- Low contact resistivity at the (contact) metal/semiconductor interface [13]: The low solubility of boron in Si was shown to be a limiting factor for the contact of  $\text{p}^+$ -poly-Si layers with conventional furnace-processed layers [14].
- Maskless and, consequently, low-cost patterning: Highly boron-doped  $\text{p}^{++}$ -poly-Si layers provide the necessary etch stop in an alkaline solution such as potassium hydroxide (KOH) [15]. We currently use this feature for the production of advanced passivated contact cells with selective  $\text{p}^{++}$ -poly-Si layers [16,17].

Thus, the high active boron concentration in the poly-Si of the stack  $\text{p}^{++}$ -poly-Si/ $\text{SiO}_2$ /bulk Si has many advantages. However, there are two main open questions:

- How stable is the high supersaturated active boron concentration achieved by laser activation during solar processing, particularly in high-temperature processes such as subsequent furnace diffusion, oxidation, or high-temperature annealing? Other authors have studied *boron-implanted*, laser-annealed, highly boron-doped poly-Si layers and demonstrated reduced electrical activity after such annealing processes: dopant clustering or precipitation was deemed responsible [18–20]. Mizushima et al. showed that boron precipitation also happens after high-temperature annealing in highly boron-doped a-Si layers deposited via a low-pressure chemical vapor deposition (LPCVD) method [21]. Some studies also showed that boron atoms segregate at poly-Si grain boundaries, resulting in electrically inactive boron atoms [22,23]. A similar effect was also previously observed for dopant-implanted and laser-annealed samples with other dopants, such as phosphorus and arsenic [24,25].
- What is the surface passivation quality of  $\text{p}^{++}$ -poly-Si/ $\text{SiO}_2$  passivation stacks with highly boron-doped poly-Si layers? High open-circuit voltages are indispensable for highly efficient solar cells.

The present contribution reports on an extensive thermal stress test of our highly laser-doped, supersaturated poly-Si layers by measuring the conductivity after high-temperature annealing steps 30 min in length. In addition, in parallel, we investigated

the passivation quality of the SiO<sub>2</sub>/bulk Si interface by monitoring the implied open-circuit voltage derived from minority carrier lifetime measurements. Our main results are as follows:

- The classic deposition of passivating SiN<sub>x</sub>:H at a moderate deposition temperature  $T_{\text{depo.}} = 450\text{ }^{\circ}\text{C}$  for  $t_{\text{depo.}} = 30\text{ min}$  and with fast firing with a short exposure time (several seconds) to a high peak temperature  $T_{\text{firing}} = 825\text{ }^{\circ}\text{C}$  does *not* reduce the conductivity of the laser-activated/doped poly-Si.
- The high (electrically active) boron concentrations obtained with laser activation are *significantly* reduced during high-temperature annealing steps with temperatures in the range  $600\text{ }^{\circ}\text{C} \leq T_{\text{anneal}} \leq 1000\text{ }^{\circ}\text{C}$  and relatively long annealing times  $t_{\text{anneal}} = 30\text{ min}$ . However, this effect is only due to a reduction in/the deactivation of electrically active boron atoms during high-temperature annealing, not due to out-diffusion. As a consequence, here, we introduce a novel laser *reactivation* process by melting the poly-Si a second time. This process “heals” the poly-Si layers again and almost completely re-establishes the high boron concentrations with high sheet conductances  $G_{sh}$  up to  $G_{sh} = 24\text{ mS sq.}$
- High (implied) open-circuit voltages after the original laser activation require high-temperature annealing (which, at the same time, degrades the conductivity of poly-Si). However, using our novel laser reactivation process not only restores the original high conductivity but also is compatible with high passivation quality. Finally, together with the high sheet conductance  $G_{sh} = 24\text{ mS sq.}$  we also obtain an implied open-circuit voltage  $iV_{OC} = 715\text{ mV.}$

Thus, our novel process, consisting of the laser activation (doping) of highly boron-doped poly-Si, thermal annealing (to improve the passivation quality of the SiO<sub>2</sub>/bulk Si interface) and laser *re-activation*, paves the road to highly efficient tunnel oxide passivated solar cells using p<sup>+</sup>-poly-Si/SiO<sub>2</sub> stacks on bulk Si.

## 2. Sample Preparation

Figure 1 shows the process flow to create the test samples for studying the effect of high-temperature annealing on the electrical characteristics and passivation quality of laser-activated p<sup>+</sup>-poly-Si/SiO<sub>2</sub> layers. We used as-cut n-type Czochralski (Cz) silicon substrates with a base resistivity of 3.4 Ωcm. Wafers were saw-damage-etched in a sodium hydroxide (NaOH) solution and cleaned in a mixture of sulfuric acid (H<sub>2</sub>SO<sub>4</sub>) and hydrogen peroxide (H<sub>2</sub>O<sub>2</sub>). Next, we used a tube process to thermally oxidize the wafers to create a thin interfacial oxide layer with a thickness of approximately 2 nm. Afterward, we used LPCVD to deposit a hydrogen-free intrinsic silicon thin film with a thickness of around 150 nm. Next, we lightly doped these films in a boron tribromide (BBr<sub>3</sub>) diffusion furnace at a diffusion temperature  $T_{\text{diff}} = 820\text{ }^{\circ}\text{C}$ . This high-temperature step also recrystallizes the silicon thin film. A grain size of  $d_g \approx 6\text{ nm}$  was extracted using a peak analysis of X-ray diffraction (XRD) measurements after the BBr<sub>3</sub> diffusion step. The borosilicate glass (BSG) created during diffusion was removed in 2% hydrofluoric acid (HF) prior to the laser activation process. Laser activation was performed on nine square-shaped fields with an area  $A_{\text{laser-field}} = 38 \times 38\text{ mm}^2$  with a green nanosecond laser tool and a rectangular-shaped top-hat laser beam profile with an area of  $A_{\text{spot}} = 300 \times 600\text{ }\mu\text{m}^2$ . All fields were processed with the same laser pulse energy density  $H_p = 2.1\text{ J/cm}^2$ . This  $H_p$  value, in our previous publication, was found to be the optimal laser processing setting for our poly-Si layer with a thickness of  $d_{\text{poly-Si}} = 150\text{ nm}$  [8]. The irradiation was performed with the same pulse repetition rate of  $f = 16\text{ kHz}$ . The laser pulse overlap was 10% in both scanning directions (x,y). An average grain size of  $d_g \approx 20\text{ nm}$  was extracted from the XRD measurements after laser activation. The electrical properties of the samples were measured at this stage by a four-point-probe measurement of the sheet resistance  $R_{sh}$  and electrochemical capacitance–voltage profiling (ECV) for the characterization of the doping profile.

Subsequently, the laser-activated samples were annealed at different temperatures, ranging from  $T_{\text{anneal,min}} = 600\text{ }^{\circ}\text{C}$  to  $T_{\text{anneal,max}} = 1000\text{ }^{\circ}\text{C}$ , in nitrogen ambient for a duration

of  $t_{\text{anneal}} = 30$  min using six wafers per annealing temperature. Subsequently, the annealed samples at different temperatures were divided into two main groups, each consisting of three wafers:

- Sheet resistance samples: These samples were used to study the effect of different annealing temperatures on the electrical properties. The  $R_{sh}$  and the doping profiles of this group were measured after high-temperature annealing. The second laser reactivation and healing process was carried out for this group, followed by additional  $R_{sh}$  and ECV measurements.
- Passivation samples: We used these symmetrical samples to assess the influence of each annealing temperature on the passivation quality. For this purpose, using plasma-enhanced chemical vapor deposition (PECVD), both the front and rear sides of these samples were coated with a silicon nitride ( $\text{SiN}_x\text{:H}$ ) layer, which serves as a hydrogen source for improving the passivation by the saturation of defects at/in the interfacial oxide. The passivation quality was measured with quasi-steady-state photoconductance (QSSPC) measurement using a Sinton WCT-120 tool. Additionally, we used photoluminescence (PL) imaging for the qualitative assessment of the passivation.

The passivation quality following the laser reactivation step was not tested with the indicated sheet resistance samples due to the destructive nature of the ECV measurement. Instead, as described in Section 6, we created a new set of samples to investigate the influence of the laser reactivation step on passivation with different laser pulse energy densities.

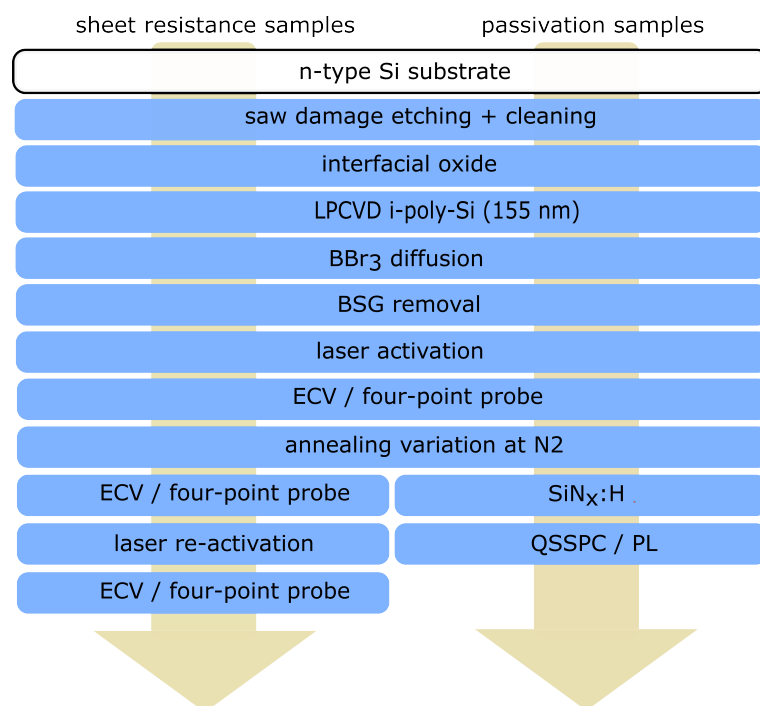


**Figure 1.** The process flow for test sample preparation. After the saw damage etching and cleaning of the substrates, the  $\text{SiO}_2$ /i-poly-Si layers were symmetrically created on the front and rear of the wafers. Next, the intrinsic Si films were lightly doped in a  $\text{BBr}_3$  diffusion furnace. After removing the BSG layer, the laser activation step was performed. Here, the electrical characteristics of samples were measured prior to the annealing variation step. Next, the samples were annealed in nitrogen ambient at different annealing temperatures for a duration of  $t_{\text{anneal}} = 30$  min. Thereafter, samples were split into two groups: sheet resistance samples and passivation samples. Sheet resistance samples were used to measure the doping profile and  $R_{sh}$  after the annealing variation step. This group of samples received the second laser reactivation (and healing) and subsequent  $R_{sh}$  and ECV measurements. The passivation samples received an extra  $\text{SiN}_x\text{:H}$  layer before the QSSPC and PL measurements.

### 3. Deactivation

The industrial production of screen-printed passivated contact solar cells usually involves several high-temperature steps, such as high-temperature annealing, SiN<sub>x</sub>:H deposition, and a fast-firing step [4,5]. In our case, this raises the question of the stability of our high active boron concentration, achieved by non-equilibrium, laser-induced supersaturation, during these thermal processes. Consequently, we performed a detailed study on the temperature-induced stress resistance of the laser-doped/activated poly-Si layers.

#### 3.1. Deactivation during SiN<sub>x</sub>:H Deposition and Fast Firing

Most of the current industrial c-Si solar cells use a PECVD-based SiN<sub>x</sub>:H coating as an antireflection (AR) layer and hydrogen source for passivation [26]. To imitate the real solar cell process with SiN<sub>x</sub>:H deposition at the front and rear, we annealed the laser-activated samples twice in a PECVD furnace at  $T_{\text{depo.}} = 450 \text{ }^\circ\text{C}$  for  $t_{\text{depo.}} = 30 \text{ min}$  without SiN<sub>x</sub>:H deposition.

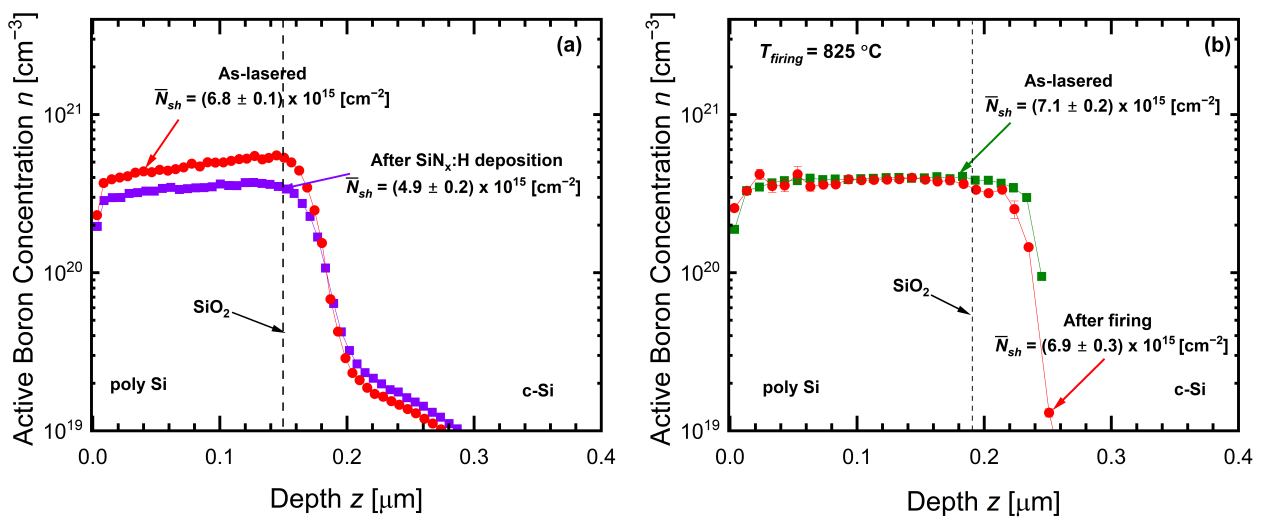
Deactivation during the fast-firing step was also tested by measuring the ECV profiles of a laser-activated sample before and after fast firing at a  $T_{\text{firing}} = 825 \text{ }^\circ\text{C}$  peak temperature.

Figure 2a compares the ECV profiles of samples after the laser process and after the annealing step under the SiN<sub>x</sub>:H deposition condition. We quantified the reduction in the active boron concentration by comparing the depth-integrated average active doping dose or sheet concentration ( $\bar{N}_{sh}$ ) within the poly-Si layers.  $\bar{N}_{sh}$  is calculated by integrating the ECV profiles over the poly-Si layer thickness using

$$\bar{N}_{sh} = \int_0^{d_{\text{poly-Si}}} n(z) dz. \quad (1)$$

Even though the sheet concentration is reduced from  $\bar{N}_{sh} = (6.8 \pm 0.1) \times 10^{15} \text{ cm}^{-2}$  to  $\bar{N}_{sh} = (4.9 \pm 0.2) \times 10^{15} \text{ cm}^{-2}$  after the annealing step at SiN<sub>x</sub>:H deposition condition, the sheet concentration is still in a good range for establishing a metal/semiconductor contact with low contact resistivity [27].

Figure 2b shows the effect of the fast-firing step on the active doping concentration of a laser-processed poly-Si layer. The sheet concentration is almost unaffected by the fast-firing step, with a measured  $\bar{N}_{sh} = (7.1 \pm 0.2) \times 10^{15} \text{ cm}^{-2}$  for the as-lasered stage and  $\bar{N}_{sh} = (6.9 \pm 0.3) \times 10^{15} \text{ cm}^{-2}$  after fast firing.



**Figure 2.** (a) Dopant deactivation for simulated (double) SiN<sub>x</sub>:H deposition. The laser-processed samples were annealed twice at  $T_{\text{depo.}} = 450 \text{ }^\circ\text{C}$  for  $t_{\text{depo.}} = 30 \text{ min}$  to mimic SiN<sub>x</sub>:H deposition on the front and rear sides of a solar cell. The annealing steps result in a slight reduction in the active doping concentration. (b) The active doping concentration in the laser-processed poly-Si layer remain almost unchanged after the fast-firing step with a peak temperature  $T_{\text{firing}} = 825 \text{ }^\circ\text{C}$ .

### 3.2. Deactivation during High-Temperature Annealing

Figure 3a shows the sheet conductance of the samples directly after the first laser activation and after annealing at various temperatures. To acquire the  $G_{sh}$  values, the sheet resistance of the samples was measured at three points of each of nine laser-activated fields and then converted to  $G_{sh}$  values through

$$G_{sh} = 1/R_{sh}. \quad (2)$$

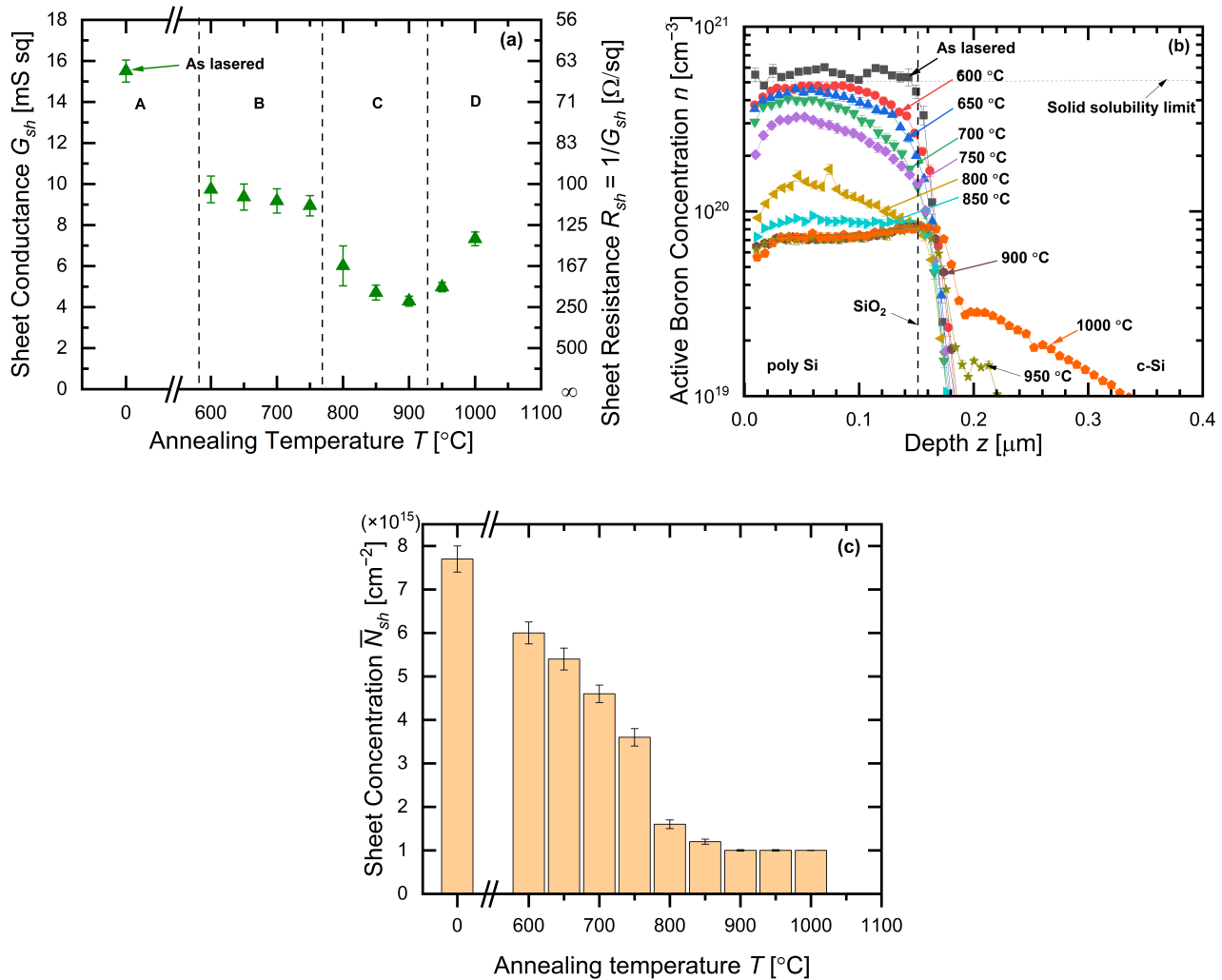
The substrates of the samples do not contribute to the  $G_{sh}$  values because of the use of opposite doping types for substrates and poly-Si layers (See Figure 1).

We categorize the  $G_{sh}$  values into four zones based on the observed differences in the dependency of  $G_{sh}$  on annealing temperature:

- **Zone A,  $T_{\text{anneal}} = 0$  °C:** Without annealing, high  $G_{sh} = 15$  mS sq is measured after laser activation.
- **Zone B,  $600$  °C  $\leq T_{\text{anneal}} \leq 750$  °C:** Annealing the laser-activated layers results in a reduction in the conductivity from  $G_{sh} = 15$  mS sq for the as-lasered stage to  $G_{sh} = 10$  mS sq for samples annealed at  $T_{\text{anneal,min}} = 600$  °C. But increasing the annealing temperature only marginally reduces  $G_{sh}$ , with a deactivation rate  $D_r = 5 \times 10^{-6}$  mS sq/°C up to  $T_{\text{anneal}} = 750$  °C.
- **Zone C,  $750$  °C  $< T_{\text{anneal}} \leq 900$  °C:** Annealing in this range results in a significant reduction in  $G_{sh}$  values; the deactivation rate is  $D_r = 1.2 \times 10^{-5}$  mS sq/°C. The minimum  $G_{sh} = 4$  mS sq is obtained for samples annealed at  $T_{\text{anneal}} = 900$  °C. This temperature range is also relevant for poly-Si annealing in passivated contact solar cells. Hence, the observed deactivation might create problems in today's real solar cell production. In the same temperature range, an earlier study [18] also found substantial deactivation for boron-implanted and laser-annealed samples. Boron precipitation was assumed to be responsible for the deactivation [18].
- **Zone D,  $T_{\text{anneal}} > 900$  °C:** The  $G_{sh}$  values increase when increasing the annealing temperature at a rate of  $D_r = 4.7 \times 10^{-5}$  mS sq/°C. We attribute this fact to the creation of a doping tail inside the c-Si substrate, as shown by the ECV profiles in Figure 3b.

Figure 3b compares the electrically active doping profiles of samples after laser activation and after different annealing steps. The ECV profiles follow the trend of  $G_{sh}$  values in different zones, as defined in Figure 3a. For non-annealed samples (temperature zone A), after the laser activation step, high active boron concentrations are measured that exceed the solid solubility limit of boron in Si  $s_{\text{max}} \approx 5 \times 10^{20}$  cm<sup>-3</sup> at 1200 °C [28]. The flat, box-shaped profile shows that the electrically active boron atoms are distributed homogeneously in the entire poly-Si layer after laser activation. For  $600$  °C  $\leq T_{\text{anneal}} \leq 750$  °C, in temperature zone B, after annealing at  $T_{\text{anneal}} = 600$  °C, the ECV profile shifts to lower concentrations, and it evolves from a flat profile (for the lasered stage) to a curved profile (after annealing). The main reduction in the active concentration is observed at the surface as well as at the poly-Si/SiO<sub>2</sub> interface. In this temperature zone (B), increasing the annealing temperature leads to a continuous shift in the active concentration to lower values. Also, the deactivation at the surface and at the poly-Si/SiO<sub>2</sub> interface becomes more pronounced at higher annealing temperatures. This fact suggests that deactivation in this temperature zone occurs via the segregation and deactivation of boron atoms into the native SiO<sub>2</sub> at the surface of the poly-Si layer as well as into the interfacial SiO<sub>2</sub> at the poly-Si/SiO<sub>2</sub> interface. For annealing temperatures in the range  $750$  °C  $< T_{\text{anneal}} \leq 900$  °C, in temperature zone C, significant deactivation occurs at  $T_{\text{anneal}} = 800$  °C. We assume that boron precipitation occurs at this temperature range, as suggested by Ref. [18]. Higher annealing temperatures further reduce the active boron concentration and result in relatively flat profiles. In temperature zone D, for temperatures  $T_{\text{anneal}} \geq 950$  °C, the doping tail extends into the c-Si mono crystalline substrate. The tail becomes deeper when increasing the annealing temperature. The observed effect depends

on the thickness of the interfacial SiO<sub>2</sub>. The thickness of the interfacial SiO<sub>2</sub> determines the amount of doping tail extension into the c-Si bulk.



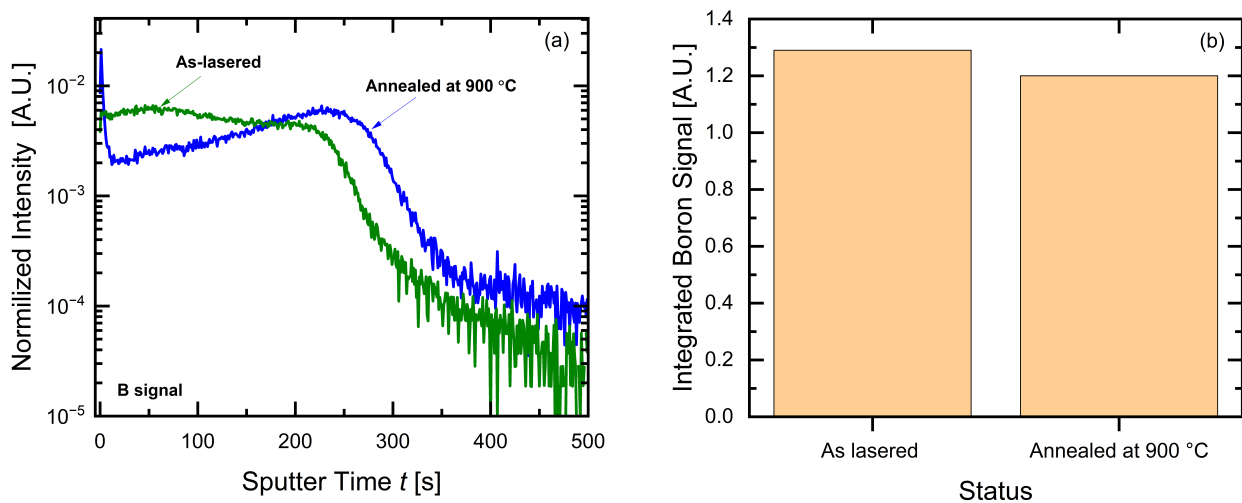
**Figure 3.** (a) The high  $G_{sh}$  obtained after laser activation in zone A is reduced to the lower  $G_{sh}$  value when performing the different annealing steps in temperature zone B. However, in zone B,  $G_{sh}$  only shows a minor reduction at higher annealing temperatures. In temperature zone C,  $T_{\text{anneal}} = 800$  °C results in another significant decrease in  $G_{sh}$ , and deactivation occurs at a higher rate in this zone compared to zone B. Annealing temperatures  $T_{\text{anneal}} \geq 950$  °C in temperature zone D raise the conductivity once again by deepening the doping tail in the c-Si substrate, as proven by ECV measurements. (b) The high boron concentration after laser activation continuously decreases when increasing the annealing temperature up to  $T_{\text{anneal}} = 750$  °C. The reduction in concentration is more pronounced at the poly-Si layer's surfaces as well as at the poly-Si/SiO<sub>2</sub> interfaces. The  $800$  °C  $\leq T_{\text{anneal}} \leq 900$  °C temperature range significantly lowers the concentration. At higher annealing temperatures of  $T_{\text{anneal}} = 950$  °C and  $T_{\text{anneal}} = 1000$  °C, the boron concentration within the poly-Si layer remains at the lowest measured level, whereas the created doping tail in the c-Si substrate gets deeper when increasing the annealing temperature. The doping tail in c-Si contributes to the measured sheet resistance, and therefore, as shown in (a), it raises the conductance. (c) The active doping dose in the poly-Si layer decreases from  $\bar{N}_{sh} = (7.7 \pm 0.3) \times 10^{15} \text{ cm}^{-2}$  to  $\bar{N}_{sh} = (6 \pm 0.2) \times 10^{15} \text{ cm}^{-2}$  after annealing the laser-activated samples at  $T_{\text{anneal}} = 600$  °C, demonstrating electrical deactivation upon high-temperature annealing. Further reductions in  $\bar{N}_{sh}$  continue for samples annealed at higher temperatures up to  $T_{\text{anneal}} = 900$  °C. Annealing temperatures  $T_{\text{anneal}} \geq 900$  °C do not further decrease the active doping dose in the poly-Si layer.

Figure 3c depicts the sheet concentration  $\bar{N}_{sh}$  within the poly-Si layer. As expected from the ECV profiles,  $\bar{N}_{sh}$  decreases continuously when increasing the annealing temperature up to  $T_{anneal} = 900$  °C, where  $\bar{N}_{sh}$  stabilizes at the minimum value. The doping tail created inside the c-Si bulk for  $T_{anneal} > 900$  °C is not considered in  $\bar{N}_{sh}$  determination.

### 3.3. ToF-SIMS Profiles

Figure 4a compares the boron signals of a Time-of-Flight secondary ion mass spectrometry (ToF-SIMS) measurement after laser activation and after annealing at  $T_{anneal} = 900$  °C. The measurements were performed with a TOF.SIMS V from the company IONTOF GmbH. The flat profile after laser activation shows the uniform distribution of boron atoms within the poly-Si layer. The annealing step redistributes boron atoms in the poly-Si layer and increases the concentration directly at the surface and toward the poly-Si/SiO<sub>2</sub> interface, which is explained by boron segregation in native SiO<sub>2</sub> at the surface and in interfacial SiO<sub>2</sub>. The segregated boron atoms become electrically deactivated, supporting the detected deactivation at the poly-Si surface and poly-Si/SiO<sub>2</sub> interface in the ECV profiles shown in Figure 3b.

Figure 4b depicts the integrated boron signals over the sputtering time for samples after laser activation and after annealing at  $T_{anneal} = 900$  °C. Unlike the significant active boron concentration loss observed after annealing at  $T_{anneal} = 900$  °C in the ECV profiles in Figure 3b, the integral of the ToF-SIMS profiles only exhibits a marginal reduction in the overall boron concentration after the annealing step, implying that boron atoms are still present in the poly-Si layer.



**Figure 4.** (a) After the laser activation step, boron atoms are distributed homogeneously in the poly-Si layer, creating a relatively flat ToF-SIMS profile. After annealing at  $T_{anneal} = 900$  °C, the boron concentration is increased at the surface of the poly-Si layer as well as at the poly-Si/SiO<sub>2</sub> interface, which indicates the possible segregation of the boron atoms into native SiO<sub>2</sub> at the poly-Si surface and interfacial SiO<sub>2</sub>. (b) Integrating the boron signal over the sputtering time shows similar amounts of boron atoms after laser activation and after the annealing step. This finding indicates that boron atoms do not out-diffuse during the annealing step and are still present in the poly-Si layer.

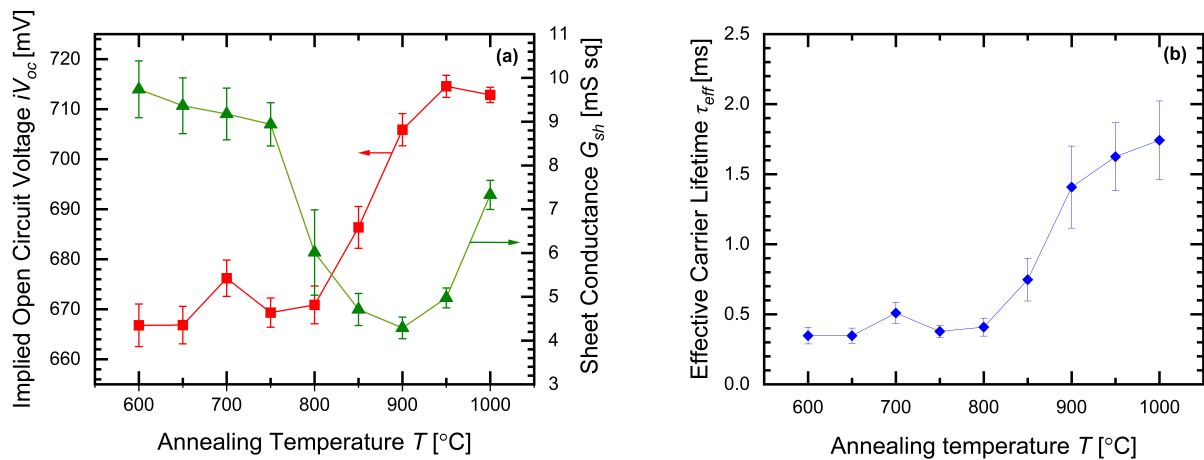
## 4. Passivation

Figure 5a shows the passivation quality of the lifetime samples in terms of  $iV_{OC}$  at different annealing temperatures. The  $G_{sh}$  values from Figure 3a are also shown to illustrate the trade-off between the conductivity and passivation quality of the p<sup>++</sup>-poly-Si/SiO<sub>2</sub> layers. We derived the  $iV_{OC}$  values from the QSSPC measurement of nine laser-activated fields using the Sinton WCT-120 tool [29]. The measured  $iV_{OC}$  starts to increase when elevating the annealing temperature from  $T_{anneal} > 800$  °C until it reaches the highest  $iV_{OC} = (714 \pm 2)$  mV at  $T_{anneal} = 950$  °C. This result is compatible with other studies [30,31],

which showed that the passivation quality of poly-Si/SiO<sub>2</sub> layers strongly depends on the annealing temperature. The improved passivation is mainly attributed to increased field-effect passivation due to the dopant diffusing into the substrate and forming a pn junction, resulting in the repelling of one carrier type. Additionally, Liu et al. showed that high-temperature annealing reconstructs the interfacial SiO<sub>2</sub> and reduces the acceptor-like defects from oxygen atoms [32]. It also seems plausible that SiO<sub>2</sub> needs to be annealed after possibly being impaired by the Si melt during the laser activation step. The higher annealing temperature  $T_{\text{anneal}} = 1000$  °C results in the degradation of passivation, and therefore, a lower  $iV_{OC}$  value is measured for these samples. We attribute the passivation loss in  $T_{\text{anneal}} = 1000$  °C to the damaged SiO<sub>2</sub> and the deep diffusion of boron into the c-Si substrate, as shown in Figure 3b. The created doping tail inside the substrate increases the conductance; however, the active boron concentration within the poly-Si layer remains at the lowest measured level (see Figure 3b).

Even though the best passivation quality is achieved at  $T_{\text{anneal}} = 950$  °C, samples annealed at this temperature show a low sheet conductance of  $G_{sh} = (5 \pm 0.2)$  mS sq. Due to the trade-off between the passivation quality and the conductivity of the p<sup>++</sup>-poly-Si/SiO<sub>2</sub> layers shown in Figure 5a, an alternative process is needed if the high supersaturated, electrically active boron concentrations need to be maintained after annealing, e.g., for low contact resistivities.

Figure 5b shows the effective carrier lifetime  $\tau_{\text{eff}}$  measured at a minority carrier density of  $1 \times 10^{15}$  cm<sup>-3</sup>.  $\tau_{\text{eff}}$  follows the same trend as  $iV_{OC}$  values and starts to increase at  $T_{\text{anneal}} > 800$  °C, showing that the high-temperature annealing step is necessary to achieve a high passivation quality with a high carrier lifetime.



**Figure 5.** (a) Trade-off for the sheet conductance  $G_{sh}$  and implied open-circuit voltage  $iV_{OC}$  for different annealings of the p<sup>++</sup>-poly-Si/SiO<sub>2</sub> layers. For  $T_{\text{anneal}} \leq 800$  °C, a poor passivation quality with low  $iV_{OC}$  is measured. Increasing the annealing temperature to  $T_{\text{anneal}} \geq 800$  °C, on the one hand, improves  $iV_{OC}$  (shown by the left y-axis and indicated by the red arrow), but, on the other hand, the  $G_{sh}$  is reduced (shown by the right y-axis and indicated by the green arrow). (b) The effective carrier lifetime  $\tau_{\text{eff}}$  dependency on the annealing temperature. As suggested by the  $iV_{OC}$  values in (a), high annealing temperatures  $T_{\text{anneal}} > 800$  °C are required to obtain high  $\tau_{\text{eff}}$  values.

## 5. Laser Reactivation as Healing Process

Figure 6a compares  $G_{sh}$  values of thermally deactivated, annealed samples with those of samples after healing with a laser reactivation step. For the reactivation, we performed a second laser process with  $H_p = 2$  J/cm<sup>2</sup> using the laser tool described in Section 2. For all deactivated samples at the various annealing temperatures, the second, healing laser irradiation raises the conductivity to  $G_{sh}$  values similar to those of samples without the thermal deactivating annealing step. The high  $G_{sh}$  of the reactivated samples previously annealed at  $T_{\text{anneal}} = 1000$  °C is ascribed to the combination of conductance from the high

boron concentration within the poly-Si layer after reactivation and the conductance from the deep doping tail in the c-Si substrate (see Figure 3b).

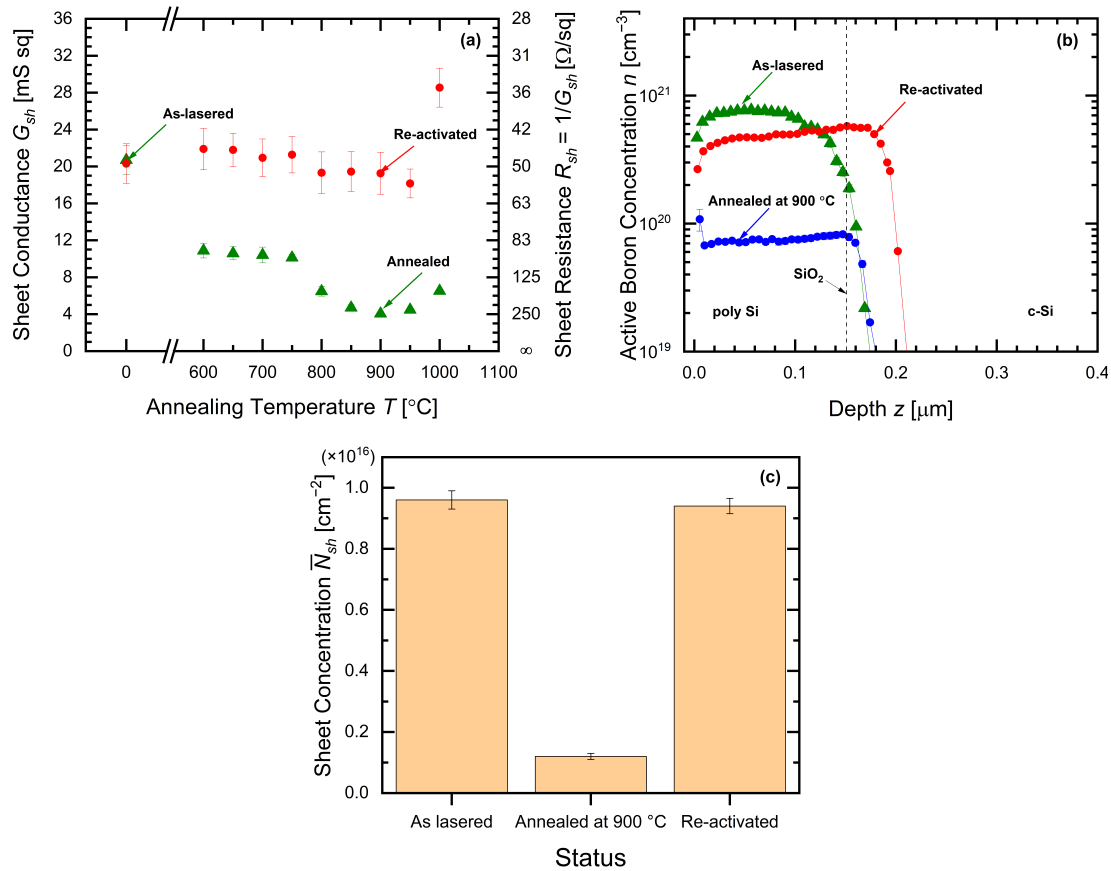


**Figure 6.** (a) The second, healing, reactivating laser treatment of the thermally annealed and deactivated samples increases the conductivity of the poly-Si layers to that in the as-lasered stage, regardless of the level of deactivation caused by different annealing temperatures. The pronounced diffusion of boron atoms into the c-Si substrate at  $T_{\text{anneal}} = 1000$  °C contributes to the conductance and results in higher  $G_{sh}$  after reactivation compared to the samples annealed at lower annealing temperatures. (b) Due to dopant precipitation as well as segregation in  $\text{SiO}_2$ , the high active boron concentration achieved with the laser activation step is reduced to a lower concentration. The second reactivating laser treatment re-melts the poly-Si layer and, therefore, redistributes the electrically deactivated boron atoms in the Si melt, resulting again in a high electrically active boron concentration after recrystallization. (c) The similar  $\bar{N}_{sh}$  values of as-lasered and reactivated samples indicate that the total boron concentration in the poly-Si layers remains nearly unchanged after thermal annealing at  $T_{\text{anneal}} = 900$  °C. The detected reduction in  $\bar{N}_{sh}$  is solely due to the reduced concentration of electrically active boron atoms in the poly-Si layer after the annealing step.

Figure 6b shows the ECV profiles after laser activation, annealing at  $T_{\text{anneal}} = 900$  °C, and the healing reactivation step. As discussed above, the laser activation results in boron-supersaturated poly-Si layers. However, high-temperature thermal annealing reduces the active boron concentration. The second, healing laser irradiation for the reactivation of the thermally annealed samples increases the active boron concentration once again. We hypothesize that the second laser irradiation step dissolves the boron precipitates created during high-temperature thermal annealing and redistributes the segregated boron atoms in surface  $\text{SiO}_2$  and interfacial  $\text{SiO}_2$ . A similar effect was also observed in other studies [33,34]. Nevertheless, the ECV profile of our healed reactivated samples differs from that of the as-lasered samples in both the concentration and measured depth. The

reactivated sample shows lower concentrations compared to the as-lasered sample, but a deeper profile is measured for the reactivated sample.

Figure 6c shows the  $\bar{N}_{sh}$  obtained after laser activation, thermal annealing, and the healing laser reactivation. The high  $\bar{N}_{sh} = (9.6 \pm 0.3) \times 10^{15} \text{ cm}^{-2}$  for as-lasered samples is significantly reduced to  $\bar{N}_{sh} = (1.2 \pm 0.1) \times 10^{15} \text{ cm}^{-2}$  after thermally annealing at  $T_{\text{anneal}} = 900 \text{ }^\circ\text{C}$  and again increased to  $\bar{N}_{sh} = (9.4 \pm 0.2) \times 10^{15} \text{ cm}^{-2}$  with the healing laser reactivation. The close agreement in the  $\bar{N}_{sh}$  values of as-lasered samples and reactivated samples shows that the out-diffusion of boron atoms during high-temperature annealing is not the reason for the measured reduction in the active boron concentration, as is also shown via the integrated ToF-SIMS profiles in Figure 4b. Not the total but only the electrical concentration of boron atoms in the annealed sample is reduced.

## 6. Highly Conductive, Well-Passivating p<sup>++</sup>-poly-Si/SiO<sub>2</sub> Layers

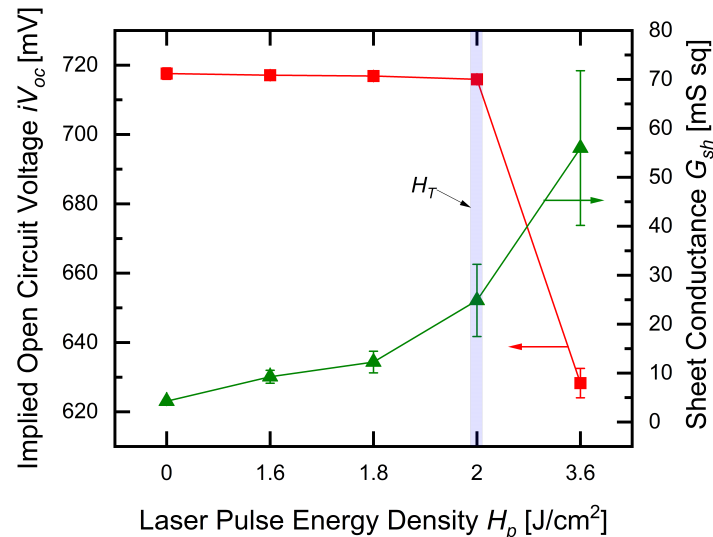
For the laser reactivation and healing step, we also examined the influence of different  $H_p$  on the passivation quality and conductivity of poly-Si/SiO<sub>2</sub> layers. For that purpose, we used the same sample preparation method as described in Section 2. For the first, original laser activation, the whole wafer was irradiated with  $H_p = 2.1 \text{ J/cm}^2$  at a  $f = 16 \text{ kHz}$  pulse repetition rate. Next, samples were annealed at  $T_{\text{anneal}} = 985 \text{ }^\circ\text{C}$  in nitrogen ambient for a duration of  $t_{\text{anneal}} = 30 \text{ min}$ . For the subsequent laser reactivation step, we irradiated the full wafer area with various  $H_p$ , with five wafers for each  $H_p$ . After  $R_{sh}$  measurements on one hundred points of each wafer, samples were covered with Aluminum Oxide (AlO<sub>x</sub>) and SiN<sub>x</sub>:H passivation layers. At this stage, we measured the  $iV_{OC}$  of the samples at five points of each wafer using the QSSPC method.

Figure 7 shows the effect of different  $H_p$  in the reactivation/healing process on the  $iV_{OC}$  and  $G_{sh}$  of the p<sup>++</sup>-poly-Si/SiO<sub>2</sub> layers. The conductivity of the layers continuously increases when increasing  $H_p$  until reaching the maximum  $G_{sh} = (56 \pm 15) \text{ mS sq}$  for the highest  $H_p = 3.6 \text{ J/cm}^2$  tested here. However,  $iV_{OC}$  significantly decreases when  $H_p$  exceeds the transition laser pulse energy density  $H_T$ , i.e., for  $H_p > H_T$ . Our previous work introduced  $H_T$  as the laser pulse energy density, which results in a melt depth equal to the poly-Si thickness [8].

In contrast to the reactivation/healing process as discussed here, our previous study [8] showed that laser energy densities  $H_p > H_T$  led to increased  $iV_{OC}$  values (in the first laser activation process). The observed difference originates from the thermal annealing step in the present process sequence (after laser activation). In the laser activation process, samples are thermally annealed *after* the laser treatment. In contrast, in the healing process using laser reactivation, samples are annealed *prior* to the (second) laser treatment and, in order to prevent another deactivation, do not receive a second, subsequent thermal annealing. We attribute the different influences of  $H_p$  on  $iV_{OC}$  in laser activation and reactivation to the effect of high-temperature annealing on the restructuring of interfacial SiO<sub>2</sub> after the laser treatment. However, avoiding the degradation of interfacial SiO<sub>2</sub>, the lack of high-temperature annealing in the reactivation process requires the precise tuning of the laser reactivation parameters.  $H_p$  in the laser reactivation step must be carefully chosen to melt the major part of the poly-Si layer thickness in the poly-Si/SiO<sub>2</sub> stack. At the same time, the created Si melt must solidify before reaching interfacial SiO<sub>2</sub>.

As detailed in Ref. [8], we found the linear dependence of the melt depth on  $H_p$  in the laser processing of the poly-Si layers, which agrees with the same finding for the conventional laser processing of bulk c-Si [35,36]. This behavior enabled us to estimate the melt depth created by different  $H_p$  [8]. For the reactivation process, we used this estimation to determine the appropriate  $H_T$  for melting the poly-Si layer in the poly-Si/SiO<sub>2</sub> stack without the Si melt damaging SiO<sub>2</sub> for different poly-Si layer thicknesses. This procedure allows us to reactivate the poly-Si layer without losing the passivation quality, resulting in a high conductivity  $G_{sh} = (24 \pm 7) \text{ mS sq}$  of the poly-Si layer together with a high  $iV_{OC} = (715 \pm 1) \text{ mV}$ , as shown in Figure 7. Such highly conductive reactivated layers with high active boron concentrations ensure low contact resistivity in the metal/semiconductor

interface [13] and enhance the lateral carrier transport through the poly-Si layer. In a separate publication, we will report on the application of these highly conductive and well-passivating  $p^{++}$ -poly-Si/SiO<sub>2</sub> layers in our advanced passivating contact solar cells.



**Figure 7.** The laser reactivation of thermally deactivated poly-Si/SiO<sub>2</sub> layers. After thermally treating originally laser-activated layers at  $T_{\text{anneal}} = 985$  °C for  $t_{\text{anneal}} = 30$  min, a low  $G_{sh} = 4$  mS sq is measured without reactivation. The reactivation process begins when the laser pulse melts the poly-Si layer at  $H_p = 1.6$  J/cm<sup>2</sup>, and the conductivity of poly-Si layers increases as  $H_p$  increases (shown by the right y-axis and indicated by the green arrow). For laser pulse energy densities below the transition fluence ( $H_p \leq H_T$ ), the Si melt recrystallizes before reaching interfacial SiO<sub>2</sub>. As a consequence, the passivation (gained by thermal annealing) is maintained, guaranteeing a constant, high  $iV_{OC} = (716 \pm 6)$  mV (shown by the left y-axis and indicated with the red arrow). For  $H_p = 3.6$  J/cm<sup>2</sup>, the (too thick) Si melt damages SiO<sub>2</sub>, resulting in passivation loss and, consequently, a lower  $iV_{OC} = (628 \pm 4)$  mV.

## 7. Conclusions

Laser doping/activation allows active boron concentrations beyond the solid solubility limit to be reached by melting the poly-Si layer in poly-Si/SiO<sub>2</sub> stacks on the Si bulk of solar cells. The rapid cooling of the Si melt traps the boron atoms in Si lattice sites, resulting in high electrically active boron concentrations and, therefore, also high conductivity. However, in the case of solar cells, the high conductivity of the poly-Si layer is not sufficient for high efficiencies: instead, the high passivation quality of the interface between SiO<sub>2</sub> and bulk Si is also necessary. According to our experimental results, high passivation quality is only possible with additional thermal annealing *after* laser activation. Typically, an annealing temperature around  $T_{\text{anneal}} = 950$  ° is necessary. Unfortunately, after such high-temperature, passivating annealing, the conductivity of the poly-Si layers is significantly reduced: the ECV profiles show a significant reduction in the originally high *electrically active* boron dose from  $\bar{N}_{sh} = (9.6 \pm 0.3) \times 10^{15}$  cm<sup>-2</sup> in the as-lasered stage to  $\bar{N}_{sh} = (1.2 \pm 0.1) \times 10^{15}$  cm<sup>-2</sup> after annealing at  $T_{\text{anneal}} = 900$  °C. In contrast, ToF-SIMS measurements only show a marginal reduction in the *total* boron concentration. This finding shows that most of the missing boron atoms are still present in the poly-Si layers: they are just deactivated by the thermal treatment. Therefore, we use a second laser treatment, a subsequent laser *reactivation* process, that re-melts the poly-Si layer again and redistributes the boron atoms once again in the Si melt, which, after recrystallization, results in raising the active dose once again to  $\bar{N}_{sh} = (9.4 \pm 0.2) \times 10^{15}$  cm<sup>-2</sup>, which is almost the same dose as before thermal deactivation. However, to maintain a high level of passivation while increasing the conductivity of the poly-Si layer, the laser pulse energy density in the

reactivation step must be carefully chosen: we have to melt the major part of the poly-Si layer without severely damaging the interfacial oxide. The laser reactivation process allows us to establish not only highly conductive poly-Si/SiO<sub>2</sub> layers with  $G_{sh} = (24 \pm 7)$  mS sq but also high passivation quality with an implied open-circuit voltage  $iV_{OC} = (715 \pm 1)$  mV. Therefore, it should also be possible to fabricate highly efficient industrial solar cells based on our new process of laser activation, thermal annealing, and, finally, laser reactivation.

**Author Contributions:** Conceptualization and experimental design, S.S.K., J.H. and J.H.W.; sample preparation, S.S.K.; measurements S.S.K., S.L. and J.L.; scientific discussion, S.S.K., J.H., S.L., J.L. and J.H.W.; writing, S.S.K.; review and editing, J.H.W., J.H., J.L. and S.L.; supervision, J.H. and J.H.W.; data analysis and visualization, S.S.K.; project administration, J.H. All authors have read and agreed to the published version of the manuscript.

**Funding:** This research was funded by Bundesministerium für Wirtschaft und Klimaschutz (BMWK), funding reference: 03EE1138A.

**Data Availability Statement:** Data is contained within the article.

**Acknowledgments:** The corresponding author also expresses gratitude to the DAAD organization for the Ph.D. scholarship. Sincere gratitude is extended to Radovan Kopecek, ISC Konstanz's managing director, for arranging the corresponding author's transfer to ISC Konstanz. We thank all of our ISC Konstanz colleagues who provided assistance with the preparation and processing of samples. We would like to thank Jan Lossen and Christoph Peter from ISC Konstanz and also Stephan Großer from Fraunhofer CSP for their insightful remarks. We also acknowledge the support of Michael Saliba, the director of ipv Stuttgart. One of us, J.H.W., is also grateful for an enlightening discussion with Antonia Salento from Puglia.

**Conflicts of Interest:** The authors declare no conflicts of interest.

## References

1. Arriaga Arruti, O.; Virtuani, A.; Ballif, C. Long-term performance and reliability of silicon heterojunction solar modules. *Prog. Photovolt. Res. Appl.* **2023**, *31*, 664–677. [CrossRef]
2. Wang, V. A Look into the 2024 PV Landscape: Top 10 PV Module Manufacturers' Capacity Plans. Available online: <https://www.solarbeglobal.com/a-look-into-the-2024-pv-landscape-top-10-pv-module-manufacturers-capacity-plans/> (accessed on 27 April 2023).
3. Kafle, B.; Goraya, B.S.; Mack, S.; Feldmann, F.; Nold, S.; Rentsch, J. TOPCon—Technology options for cost efficient industrial manufacturing. *Sol. Energy Mater. Sol. Cells* **2021**, *227*, 111100. [CrossRef]
4. Chen, Y.; Chen, D.; Liu, C.; Wang, Z.; Zou, Y.; He, Y.; Wang, Y.; Yuan, L.; Gong, J.; Lin, W. Mass production of industrial tunnel oxide passivated contacts; et al. (i-TOPCon) silicon solar cells with average efficiency over 23% and modules over 345 W. *Prog. Photovolt. Res. Appl.* **2019**, *27*, 827–834. [CrossRef]
5. Nandakumar, N.; Rodriguez, J.; Kluge, T.; Große, T.; Fondop, L.; Padhamnath, P.; Balaji, N.; König, M.; Duttgupta, S. Approaching 23% with large-area monoPoly cells using screen-printed and fired rear passivating contacts fabricated by inline PECVD. *Prog. Photovolt. Res. Appl.* **2019**, *27*, 107–112. [CrossRef]
6. Chaudhary, A.; Hoß, J.; Lossen, J.; Huster, F.; Kopecek, R.; van Swaaij, R.; Zeman, M. Screen Printed Fire-Through Contact Formation for Polysilicon-Passivated Contacts and Phosphorus-Diffused Contacts. *IEEE J. Photovolt.* **2022**, *12*, 462–468. [CrossRef]
7. Boisenko, V.E.; Yudin, S.G. Steady-state solubility of substitutional impurities in silicon. *Phys. Status Solidi (a)* **1987**, *101*, 123–127. [CrossRef]
8. Sharbaf Kalaghichi, S.; Hoß, J.; Zapf-Gottwick, R.; Werner, J.H. Laser Activation for Highly Boron-Doped Passivated Contacts. *Solar* **2023**, *3*, 362–381. [CrossRef]
9. Kodera, H. Diffusion Coefficients of Impurities in Silicon Melt. *Jpn. J. Appl. Phys.* **1963**, *2*, 212. [CrossRef]
10. Vick, G.L.; Whittle, K.M. Solid Solubility and Diffusion Coefficients of Boron in Silicon. *J. Electrochem. Soc.* **1969**, *116*, 1142. [CrossRef]
11. Poate, J.M.; Brown, W.L. Laser annealing of silicon. *Phys. Today* **1982**, *35*, 24–30. [CrossRef]
12. White, C.W.; Wilson, S.R.; Appleton, B.R.; Young, F.W. Supersaturated substitutional alloys formed by ion implantation and pulsed laser annealing of group-III and group-V dopants in silicon. *J. Appl. Phys.* **1980**, *51*, 738–749. [CrossRef]
13. Sze, S.; Lee, M. *Semiconductor Devices: Physics and Technology*; Semiconductor Devices, Physics and Technology; Wiley: Hoboken, NJ, USA, 2012; p. 239.
14. Padhamnath, P.; Nampalli, N.; Khanna, A.; Nagarajan, B.; Aberle, A.G.; Duttgupta, S. Progress with passivation and screen-printed metallization of Boron-doped monoPoly™ layers. *Sol. Energy* **2022**, *231*, 8–26. [CrossRef]

15. Buchholz, F.; Linke, J.; Hoß, J.; Chu, H.; Mihailetchi, V.; Chaudhary, A.; Arumughan, J.; Lossen, J.; Kopecek, R.; Wefringhaus, E. Local Passivating Contacts from Laser Doped P+ Polysilicon. In Proceedings of the 38th European Photovoltaic Solar Energy Conference and Exhibition, Online, 6–10 September 2021; pp. 140–143. [\[CrossRef\]](#)
16. Kopecek, R.; Buchholz, F.; Mihailetchi, V.D.; Libal, J.; Lossen, J.; Chen, N.; Chu, H.; Peter, C.; Timofte, T.; Halm, A.; et al. Interdigitated Back Contact Technology as Final Evolution for Industrial Crystalline Single-Junction Silicon Solar Cell. *Solar* **2023**, *3*, 1–14. [\[CrossRef\]](#)
17. Linke, J.; Buchholz, F.; Peter, C.; Hoß, J.; Lossen, J.; Mihailetchi, V.; Kopecek, R. Fully Passivating Contact IBC Solar Cells Using Laser Processing. In Proceedings of the 8th World Conference on Photovoltaic Energy Conversion, Milan, Italy, 26–30 September 2022; pp. 102–106. [\[CrossRef\]](#)
18. Takamura, Y.; Jain, S.H.; Griffin, P.B.; Plummer, J.D. Thermal stability of dopants in laser annealed silicon. *J. Appl. Phys.* **2002**, *92*, 230–234. [\[CrossRef\]](#)
19. Narayan, J.; Young, R.T.; White, C.W. A comparative study of laser and thermal annealing of boron-implanted silicon. *J. Appl. Phys.* **2008**, *49*, 3912–3917. [\[CrossRef\]](#)
20. White, C.W.; Narayan, J.; Young, R.T. Laser Annealing of Ion-Implanted Semiconductors. *Science* **1979**, *204*, 461–468. [\[CrossRef\]](#) [\[PubMed\]](#)
21. Mizushima, I.; Mitani, Y.; Koike, M.; Yoshiki, M.; Tomita, M.; Kambayashi, S. Precipitation of Boron in Highly Boron-Doped Silicon. *Jpn. J. Appl. Phys.* **1998**, *37*, 1171. [\[CrossRef\]](#)
22. Thompson, K.; Bunton, J.H.; Kelly, T.F.; Larson, D.J. Characterization of ultralow-energy implants and towards the analysis of three-dimensional dopant distributions using three-dimensional atom-probe tomography. *J. Vac. Sci. Technol. Microelectron. Nanometer Struct. Process. Meas. Phenom.* **2006**, *24*, 421–427. [\[CrossRef\]](#)
23. Jin, S. Boron Activation and Diffusion in Polycrystalline Silicon with Flash-Assist Rapid Thermal Annealing. Ph.D. Thesis, University of Florida, Gainesville, FL, USA, 2011.
24. Lim, S.Q.; Williams, J.S. Electrical and Optical Doping of Silicon by Pulsed-Laser Melting. *Micro* **2022**, *2*, 1–22. [\[CrossRef\]](#)
25. Goetzlich, J.; Tsien, P.; Ryssel, H. Relaxation Behavior of Metastable As and P Concentrations in Si After Pulsed and CW Laser Annealing. *MRS Online Proc. Libr. (OPL)* **1983**, *23*, 235. [\[CrossRef\]](#)
26. Cui, M.; Ma, J.; Wu, X. Multilayer SiNx:H films as passivation and anti-reflection coating for industrial PERC solar cells. *Optik* **2022**, *268*, 169841. [\[CrossRef\]](#)
27. Lohmüller, E.; Werner, S.; Hoenig, R.; Greulich, J.; Clement, F. Impact of boron doping profiles on the specific contact resistance of screen printed Ag–Al contacts on silicon. *Sol. Energy Mater. Sol. Cells* **2015**, *142*, 2–11. [\[CrossRef\]](#)
28. Trumbore, F.A. Solid solubilities of impurity elements in germanium and silicon. *Bell Syst. Tech. J.* **1960**, *39*, 205–233. [\[CrossRef\]](#)
29. Sinton, R.A.; Cuevas, A.; Stuckings, M. Quasi-steady-state photoconductance, a new method for solar cell material and device characterization. In Proceedings of the Conference Record of the Twenty Fifth IEEE Photovoltaic Specialists Conference-1996, Washington, DC, USA, 13–17 May 1996; pp. 457–460.
30. Kim, Y.J.; Kweon, I.; Min, K.; Lee, S.; Choi, S.; Jeong, K.; Park, S.; Song, H.E.; Kang, M.G.; Kim, K.H. Thermal annealing effects on tunnel oxide passivated hole contacts for high-efficiency crystalline silicon solar cells. *Sci. Rep.* **2022**, *12*, 15024. [\[CrossRef\]](#) [\[PubMed\]](#)
31. Morisset, A.; Cabal, R.; Giglia, V.; Boulineau, A.; De Vito, E.; Chabli, A.; Dubois, S.; Alvarez, J.; Kleider, J.P. Evolution of the surface passivation mechanism during the fabrication of ex-situ doped poly-Si(B)/SiOx passivating contacts for high-efficiency c-Si solar cells. *Sol. Energy Mater. Sol. Cells* **2021**, *221*, 110899. [\[CrossRef\]](#)
32. Liu, W.; Yang, X.; Kang, J.; Li, S.; Xu, L.; Zhang, S.; Xu, H.; Peng, J.; Xie, F.; Fu, J.H.; et al. Polysilicon Passivating Contacts for Silicon Solar Cells: Interface Passivation and Carrier Transport Mechanism. *ACS Appl. Energy Mater.* **2019**, *2*, 4609–4617. [\[CrossRef\]](#)
33. Narayan, J.; White, C.W. Melting phenomenon and properties of defects associated with pulsed laser irradiation. *Philos. Mag.* **1981**, *43*, 1515–1535. [\[CrossRef\]](#)
34. Narayan, J. Melting Phenomena and Interfacial Instability Associated with Laser Irradiation. *MRS Online Proc. Libr. (OPL)* **1981**, *4*, 141. [\[CrossRef\]](#)
35. Hassan, M.; Dahlinger, M.; Köhler, J.R.; Zapf-Gottwick, R.; Werner, J.H. Unified Model for Laser Doping of Silicon from Precursors. *Materials* **2021**, *14*, 2322. [\[CrossRef\]](#)
36. Esturo-Breton, A.; Ametowobla, M.; Köhler, J.; Werner, J. Laser doping for crystalline silicon solar cell emitters. In Proceedings of the 20th European Photovoltaic Solar Energy Conference, Barcelona, Spain, 6–10 June 2005; pp. 851–854.

**Disclaimer/Publisher’s Note:** The statements, opinions and data contained in all publications are solely those of the individual author(s) and contributor(s) and not of MDPI and/or the editor(s). MDPI and/or the editor(s) disclaim responsibility for any injury to people or property resulting from any ideas, methods, instructions or products referred to in the content.